Generation and characterisation of the phenoxyl-radical containing Cu(II) complex $[Cu(triaz)_2]^+$ ($triaz^-$ = O,N chelating triazole-phenolate)

Katharina Butsch, Axel Klein*, Sara Nitsche, Kathrin Stirnat, Jonathon R. Hawkett, Eric J. L. McInnes, Matthias Bauer

Electronic Supplementary Information (ESI) available:

Table SI1 Solution and refinement data of $[Cu(triaz)_2]$.
Table SI2 Bond lengths [Å] and angles [°] for $[Cu(triaz)_2]$.
Figure SI1 Crystal structure of $[Cu(triaz)_2]$, view along the *a* axis, thermal ellipsoids shown on 50% probability level, H atoms omitted for clarity.
Fig. SI2 Stereo view on $[Cu(triaz)_2]$.
Fig. SI3 Cyclic voltammogramms of Htriaz in MeCN/nBu$_4$NPF$_6$ at 298 K at 100 mV/s scan rate; potentials in V vs. $FeCp_2/FeCp_2^+$.
Fig. SI4 Cyclic voltammogramms of Htriaz in MeCN/nBu$_4$NPF$_6$ at 298 K at various scan rates; potentials in V vs. $FeCp_2/FeCp_2^+$.
Fig. SI5 Cyclic voltammogramms of $[Cu(triaz)_2]$ in MeCN/nBu$_4$NPF$_6$ at 298 K at 100 mV/s scan rate; potentials in V vs. $FeCp_2/FeCp_2^+$.
Fig. SI6 Absorption spectrum of Htriaz in MeCN (dilute solution).
Fig. SI7 Absorption spectra of $[Cu(triaz)_2]$ recorded during electrochemical reduction at –1.0 to –1.8 V in MeCN/nBu$_4$NPF$_6$ at 298 K.
Fig. SI8 Absorption spectra of reaction mixtures containing 2 eq Htriaz and 1 eq $Cu(OTf)_2$ in MeCN/toluene 5:3 using different amounts of the bases DBU (left) and tBuNH$_2$ (right) at 298 K.
Fig. SI9 Absorption spectra recorded on mixtures of various Cu^{II} salts and Htriaz/NEt_3 mixtures in MeCN/toluene 5:3 at 298 K.
Fig. SI10 Absorption spectra of the disproportionation products generated in various mixtures of MeCN/toluene, * marks the 5:3 solvent mixture at 298 K.
Fig. SI11 Absorption spectra of the disproportionation products generated in MeCN/toluene 5:3 at 298 K using different O-bases.
Fig. SI12 Q-band EPR spectrum of $[Cu(triaz)_2]$ in glassy frozen MeCN solution, recorded at 5 K (upper black line). Simulation with $g_3 = 2.324$, $g_2 = 2.059$, $g_1 = 2.059$, shown below in red.
Fig. SI13 X-band EPR spectrum of $[Cu(triaz)_2]$ in glassy frozen CH_2Cl_2 solution, recorded at 110 K (upper black line). Simulation with $g_3 = 2.28$, $g_2 = 2.054$, $g_1 = 2.054$, $A_{Cu} = 155, 15.5, 15.5$ G and $A_N = 5, 14.5, 14.5$ G shown below in red.
Fig. SI14 X-band EPR spectra recorded on a sample containing 2 eq Htriaz deprotonated with NEt_3 and 1 eq $Cu(OTf)_2$ in 5:3 MeCN/toluene at 298 K (0-60 min).
Fig. SI15 Graphic presentation of the LC-XANES fit results. The labels are explained in Table 4.

Table SI1 Solution and refinement data of [Cu(triaz)$_2$].

Formula	$C_{40}H_{44}CuN_6O_2Cl_2$	F(000)	810
f. w. /g mol^{-1}	775.26	density /g cm^{-1}	1.305
crystal system	triclinic	abs. coeff /mm^{-1}	0.731
crystal shape	needle	refl. coll.	17796
colour	green	data, restr., param.	6946, 2, 456
space group	*P*1 (No. 2)	h, k, l	–13 < h < 13
a /Å	11.238(2)		–15 < k < 15
b /Å	13.151(2)		–16 < l < 16
c /Å	13.648(2)	final R indices [I>2σ(I)]	R_1 = 0.0660, wR_2 = 0.1538
α /°	85.54(2)	R indices (all data)	R_1 = 0.1843, wR_2 = 0.2041
β /°	82.78(2)	largest diff. p. a. h. /e Å^{-3}	0.67 and –0.87
γ /°	80.88(2)		
volume /Å^3, Z	1972.2(5), 2	CCDC	862059

Table SI2 Bond lengths [Å] and angles [°] for [Cu(triaz)$_2$].

Bond lengths			
Cu1–O1	1.863(5)	C8–C9	1.38(1)
Cu1–O2	1.849(5)	C8–C13	1.54(1)
Cu1–N1	1.958(6)	C9–C10	1.40(1)
Cu1–N4	1.987(6)	C10–C11	1.38(1)
Cl1–C24	1.686(9)	C10–C17	1.53(1)
Cl2–C4	1.680(9)	C11–C12	1.40(1)
Cl3–C23	1.680(9)	C13–C14	1.55(1)
Cl4–C3	1.680(9)	C13–C15	1.54(2)
O1–C27	1.337(9)	C13–C16	1.52(1)
O2–C7	1.333(9)	C17–C18	1.53(1)
N1–N2	1.357(9)	C17–C20	1.54(1)
N1–C26	1.36(1)	C17–C19	1.55(2)
N2–C32	1.43(1)	C21–C26	1.41(1)
N2–N3	1.34(1)	C21–C22	1.43(1)
N3–C21	1.35(1)	C22–C23	1.41(1)
N4–N5	1.373(8)	C23–C24	1.34(1)
N4–C6	1.35(1)	C24–C25	1.36(1)
N5–C12	1.43(1)	C25–C26	1.40(1)
N5–N6	1.329(9)	C27–C28	1.43(1)
N6–C1	1.36(1)	C27–C32	1.41(1)
C1–C6	1.40(1)	C28–C33	1.55(1)
C1–C2	1.39(1)	C28–C29	1.38(1)
C2–C3	1.45(1)	C29–C30	1.39(1)
C3–C4	1.34(1)	C30–C37	1.52(1)
C4–C5	1.36(1)	C30–C31	1.37(1)
C5–C6	1.40(1)	C31–C32	1.38(1)
C7–C8	1.45(1)	C33–C35	1.48(2)
C7–C12	1.39(1)	C33–C36	1.50(1)
C33–C34	1.54(2)	C20–H20B	0.9600
C37–C40	1.49(2)	C20–H20C	0.9600
C37–C38	1.45(2)	C22–H22	0.9300
C37–C39	1.56(2)	C25–H25	0.9300
C2–H2	0.9300	C29–H29	0.9300
C5–H5	0.9300	C31–H31	0.9300

C9–H9	0.9300	C34–H34A	0.9600
C11–H11	0.9300	C34–H34B	0.9600
C14–H14A	0.9600	C34–H34C	0.9600
C14–H14B	0.9600	C35–H35A	0.9600
C14–H14C	0.9600	C35–H35B	0.9600
C15–H15A	0.9600	C35–H35C	0.9600
C15–H15B	0.9600	C36–H36A	0.9600
C15–H15C	0.9600	C36–H36B	0.9600
C16–H16A	0.9600	C36–H36C	0.9600
C16–H16B	0.9600	C38–H38A	0.9600
C16–H16C	0.9600	C38–H38B	0.9600
C18–H18A	0.9600	C38–H38C	0.9600
C18–H18B	0.9600	C39–H39A	0.9600
C18–H18C	0.9600	C39–H39B	0.9600
C19–H19A	0.9600	C39–H39C	0.9600
C19–H19B	0.9600	C40–H40A	0.9600
C19–H19C	0.9600	C40–H40B	0.9600
C20–H20A	0.9600	C40–H40C	0.9600
Bond angles			
O1–Cu1–O2	157.0(3)	Cl4–C3–C4	118.7(8)
O1–Cu1–N1	91.0(2)	Cl2–C4–C3	114.6(8)
O1–Cu1–N4	98.3(3)	Cl2–C4–C5	123.2(7)
O2–Cu1–N1	95.6(2)	C3–C4–C5	122.2(9)
O2–Cu1–N4	91.2(2)	C4–C5–C6	118.0(8)
N1–Cu1–N4	138.9(3)	N4–C6–C1	108.8(7)
Cu1–O1–C27	128.3(5)	N4–C6–C5	130.2(8)
Cu1–O2–C7	131.2(5)	C1–C6–C5	121.0(8)
Cu1–N1–N2	125.7(5)	O2–C7–C8	118.7(7)
Cu1–N1–C26	129.9(5)	O2–C7–C12	124.2(7)
N2–N1–C26	103.5(6)	C8–C7–C12	117.1(7)
N1–N2–N3	115.5(6)	C7–C8–C9	117.5(7)
N1–N2–C32	124.1(6)	C7–C8–C13	122.2(7)
N3–N2–C32	120.5(7)	C9–C8–C13	120.3(7)
N2–N3–C21	103.5(6)	C8–C9–C10	125.1(7)
Cu1–N4–N5	124.3(5)	C9–C10–C11	116.9(7)
Cu1–N4–C6	129.5(5)	C9–C10–C17	119.5(7)
N5–N4–C6	103.7(6)	C11–C10–C17	123.5(7)
N4–N5–N6	114.2(6)	C10–C11–C12	120.3(8)
N4–N5–C12	124.5(6)	N5–C12–C7	121.4(7)
N6–N5–C12	121.3(6)	N5–C12–C11	115.5(7)
N5–N6–C1	104.8(6)	C7–C12–C11	123.1(7)
N6–C1–C2	130.4(8)	C8–C13–C14	108.2(7)
N6–C1–C6	108.5(7)	C8–C13–C15	112.4(9)
C2–C1–C6	121.2(8)	C8–C13–C16	111.7(7)
C1–C2–C3	115.0(8)	C14–C13–C15	109.4(8)
C2–C3–C4	122.6(8)	C14–C13–C16	107.9(8)
Cl4–C3–C2	118.7(7)	C15–C13–C16	107.1(8)
C10–C17–C18	110.5(8)	C29–C30–C37	122.2(8)
C10–C17–C19	107.7(8)	C31–C30–C37	121.9(8)
C10–C17–C20	110.7(8)	C30–C31–C32	121.6(7)
C18–C17–C19	109.4(8)	N2–C32–C27	121.0(7)
C18–C17–C20	108.7(8)	N2–C32–C31	116.4(7)
C19–C17–C20	109.8(8)	C27–C32–C31	122.6(7)
N3–C21–C22	130.5(8)	C28–C33–C34	107.9(8)
N3–C21–C26	109.8(7)	C28–C33–C35	113.3(9)
C22–C21–C26	119.7(8)	C28–C33–C36	111.0(8)
C21–C22–C23	116.4(8)	C34–C33–C35	110(1)

C22–C23–C24	121.4(8)	C34–C33–C36	107(1)
Cl3–C23–C22	119.3(8)	C35–C33–C36	107.9(9)
Cl3–C23–C24	119.3(7)	C30–C37–C38	113.6(9)
Cl1–C24–C23	114.0(7)	C30–C37–C39	106.4(9)
Cl1–C24–C25	121.6(7)	C30–C37–C40	113.1(9)
C23–C24–C25	124.4(8)	C38–C37–C39	104(1)
C24–C25–C26	116.7(8)	C38–C37–C40	117(1)
N1–C26–C21	107.8(7)	C39–C37–C40	100(1)
N1–C26–C25	130.8(7)	C1–C2–H2	122.00
C21–C26–C25	121.4(7)	C3–C2–H2	123.00
O1–C27–C28	119.8(7)	C4–C5–H5	121.00
O1–C27–C32	123.4(7)	C6–C5–H5	121.00
C28–C27–C32	116.8(7)	C8–C9–H9	117.00
C27–C28–C29	117.4(7)	C10–C9–H9	117.00
C27–C28–C33	121.1(7)	C10–C11–H11	120.00
C29–C28–C33	121.5(7)	C12–C11–H11	120.00
C28–C29–C30	125.7(8)	C13–C14–H14A	109.00
C29–C30–C31	115.8(7)	C13–C14–H14B	109.00
C13–C14–H14C	109.00	C17–C20–H20A	110.00
H14A–C14–H14B	109.00	C17–C20–H20B	109.00
H14A–C14–H14C	110.00	C17–C20–H20C	109.00
H14B–C14–H14C	109.00	H20A–C20–H20B	109.00
C13–C15–H15A	109.00	H20A–C20–H20C	109.00
C13–C15–H15B	109.00	H20B–C20–H20C	109.00
C13–C15–H15C	109.00	C21–C22–H22	122.00
H15A–C15–H15B	110.00	C23–C22–H22	122.00
H15A–C15–H15C	110.00	C24–C25–H25	122.00
H15B–C15–H15C	109.00	C26–C25–H25	122.00
C13–C16–H16A	109.00	C28–C29–H29	117.00
C13–C16–H16B	109.00	C30–C29–H29	117.00
C13–C16–H16C	109.00	C30–C31–H31	119.00
H16A–C16–H16B	110.00	C32–C31–H31	119.00
H16A–C16–H16C	109.00	C33–C34–H34A	109.00
H16B–C16–H16C	109.00	C33–C34–H34B	109.00
C17–C18–H18A	109.00	C33–C34–H34C	109.00
C17–C18–H18B	109.00	H34A–C34–H34B	109.00
C17–C18–H18C	110.00	H34A–C34–H34C	109.00
H18A–C18–H18B	109.00	H34B–C34–H34C	110.00
H18A–C18–H18C	110.00	C33–C35–H35A	109.00
H18B–C18–H18C	109.00	C33–C35–H35B	109.00
C17–C19–H19A	109.00	C33–C35–H35C	109.00
C17–C19–H19B	109.00	H35A–C35–H35B	110.00
C17–C19–H19C	109.00	H35A–C35–H35C	109.00
H19A–C19–H19B	110.00	H35B–C35–H35C	109.00
H19A–C19–H19C	109.00	C33–C36–H36A	110.00
H19B–C19–H19C	109.00	C33–C36–H36B	109.00
C33–C36–H36C	109.00	C37–C39–H39B	109.00
H36A–C36–H36B	110.00	C37–C39–H39C	109.00
H36A–C36–H36C	109.00	H39A–C39–H39B	109.00
H36B–C36–H36C	109.00	H39A–C39–H39C	109.00
C37–C38–H38A	109.00	H39B–C39–H39C	109.00
C37–C38–H38B	110.00	C37–C40–H40A	109.00
C37–C38–H38C	109.00	C37–C40–H40B	109.00
H38A–C38–H38B	109.00	C37–C40–H40C	110.00
H38A–C38–H38C	109.00	H40A–C40–H40B	109.00
H38B–C38–H38C	109.00	H40A–C40–H40C	109.00
C37–C39–H39A	109.00	H40B–C40–H40C	109.00

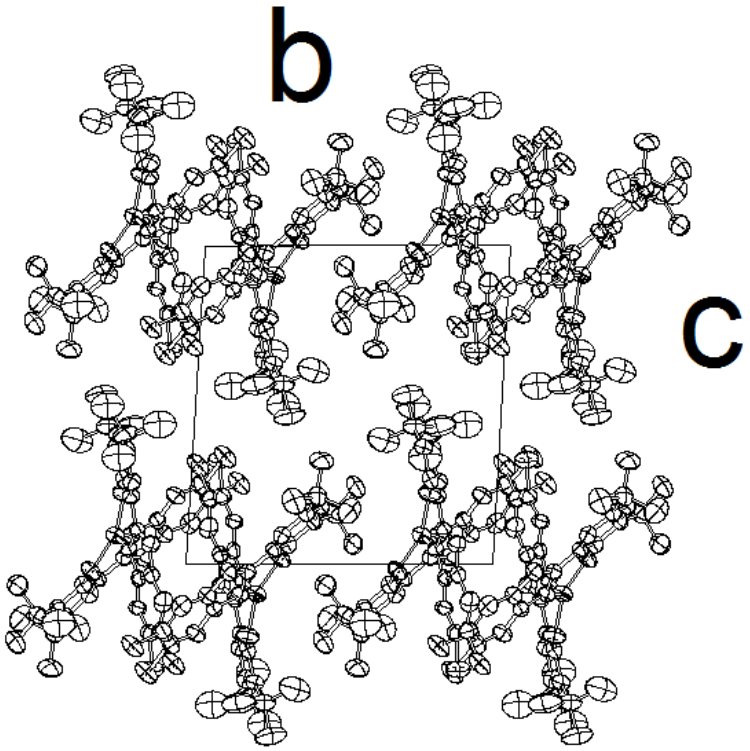

Fig. SI1 Crystal structure of [Cu(triaz)$_2$], view along the *a* axis, thermal ellipsoids shown on 50% probability level, H atoms omitted for clarity.

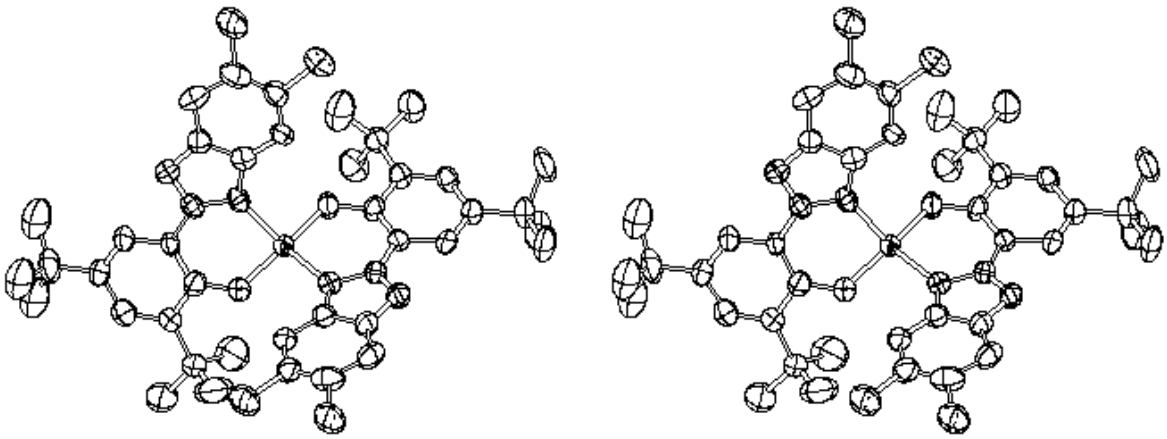

Fig. SI2 Stereo view on [Cu(triaz)$_2$].

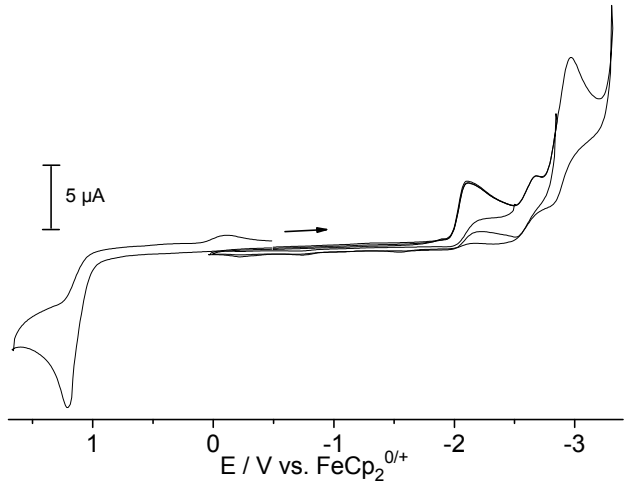

Fig. SI3 Cyclic voltammogramms of Htriaz in MeCN/nBu$_4$NPF$_6$ at 298 K at 100 mV/s scan rate; potentials in V vs. $FeCp_2/FeCp_2^+$.

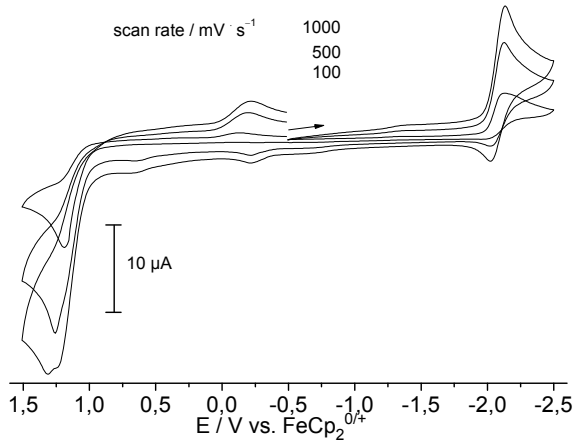

Fig. SI4 Cyclic voltammogramms of Htriaz in MeCN/nBu$_4$NPF$_6$ at 298 K at various scan rates; potentials in V vs. $FeCp_2/FeCp_2^+$.

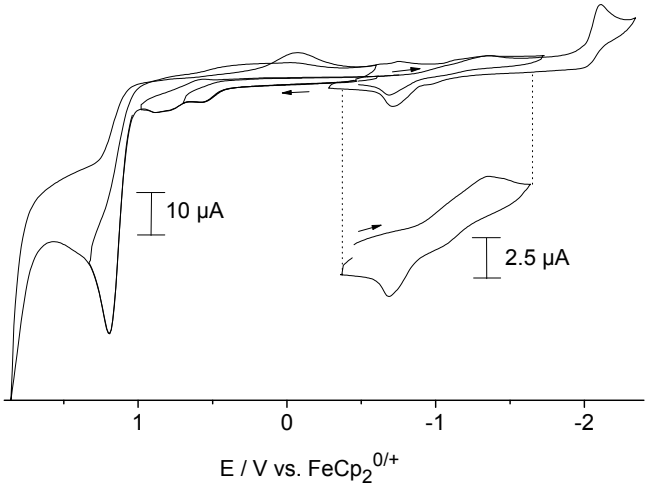

Fig. SI5 Cyclic voltammogramms of [Cu(triaz)$_2$] in MeCN/*n*Bu$_4$NPF$_6$ at 298 K at 100 mV/s scan rate; potentials in V vs. FeCp$_2$/FeCp$_2^+$, the zoomed plot at the bottom right represents the Cu(II)/Cu(I) couple.

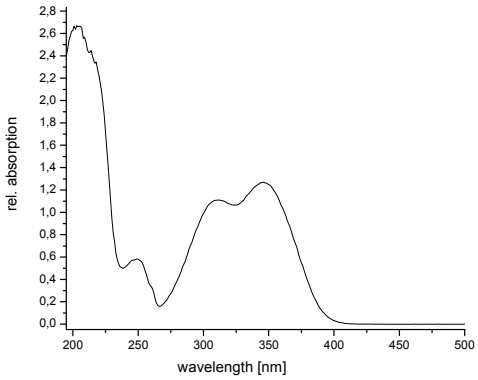

Fig. SI6 Absorption spectrum of Htriaz in MeCN (dilute solution).

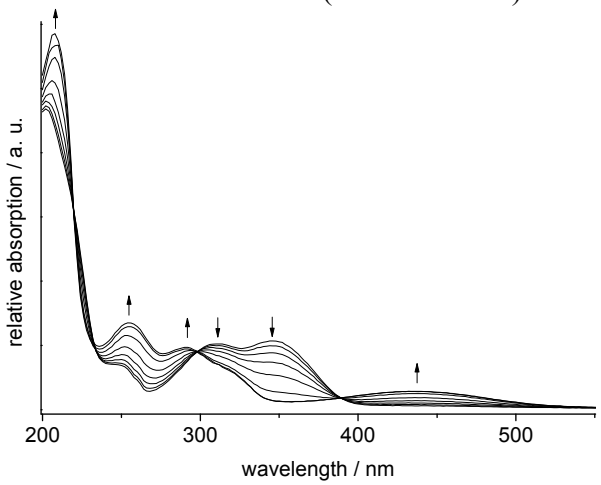

Fig. SI7 Absorption spectra of [Cu(triaz)$_2$] recorded during electrochemical reduction at 0 to –1.8 V in MeCN/*n*Bu$_4$NPF$_6$ at 298 K.

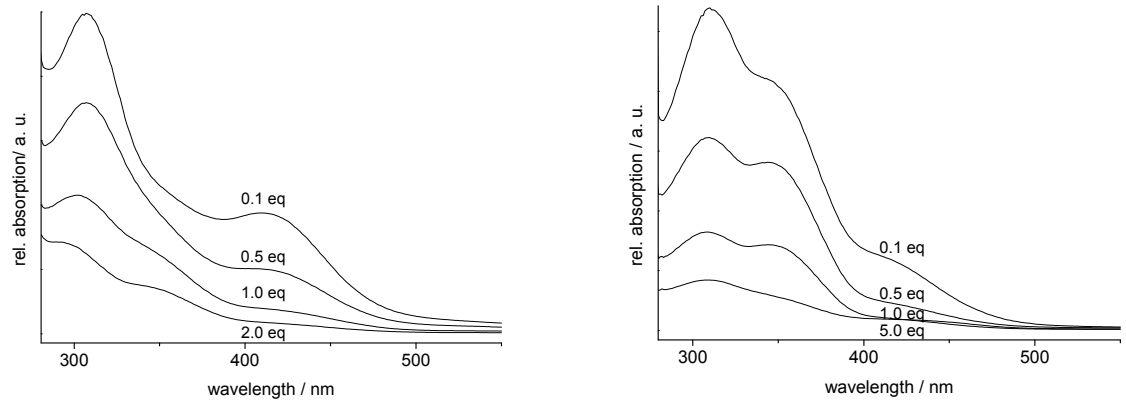

Fig. SI8 Absorption spectra of reaction mixtures containing 2 eq Htriaz and 1 eq Cu(OTf)$_2$ in

MeCN/toluene 5:3 using different amounts of the bases DBU (left) and *t*BuNH$_2$ (right) at 298 K.

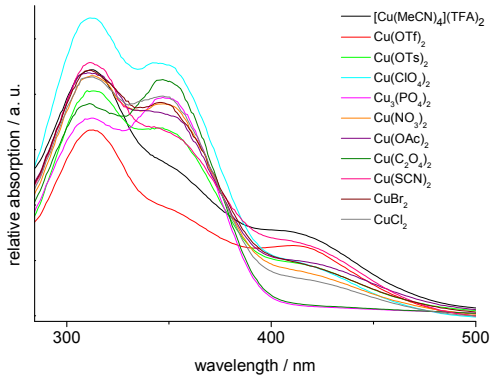

Fig. SI9 Absorption spectra recorded on mixtures of various Cu^{II} salts and Htriaz/NEt_3 mixtures in MeCN/toluene 5:3 at 298 K.

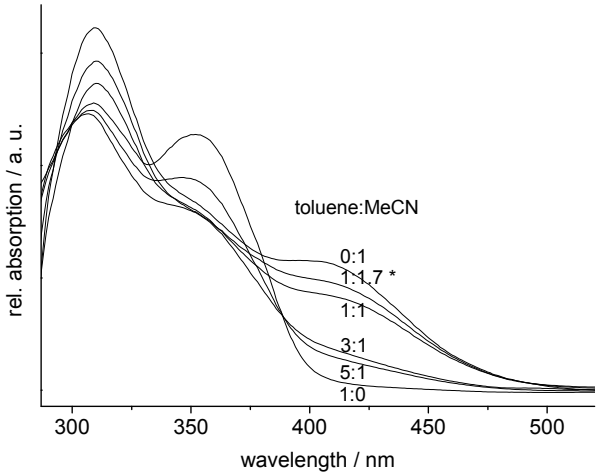

Fig. SI10 Absorption spectra of the disproportionation products generated in various mixtures of MeCN/toluene, * marks the 5:3 solvent mixture at 298 K.

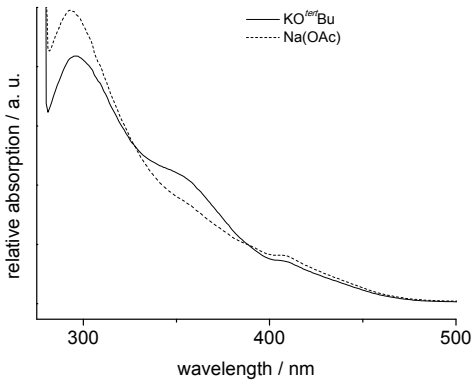

Fig. SI11 Absorption spectra of the disproportionation products generated in MeCN/toluene 5:3 at 298 K using different O-bases.

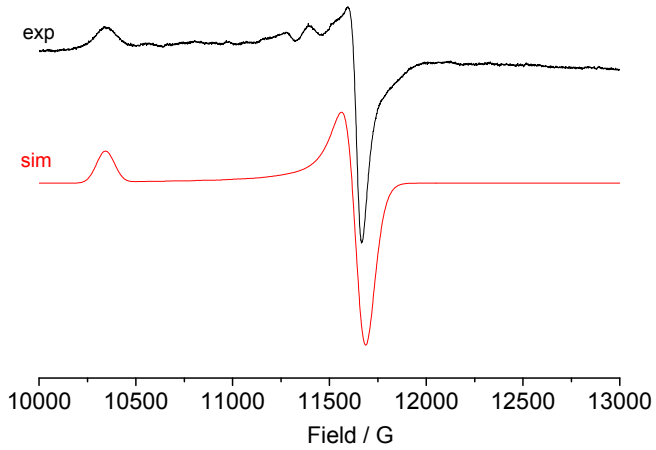

Fig. SI12 Q-band EPR spectrum of [Cu(triaz)$_2$] in glassy frozen MeCN solution, recorded at 5 K (upper black line). Simulation with $g_3 = 2.324$, $g_2 = 2.059$, $g_1 = 2.059$, shown below in red.

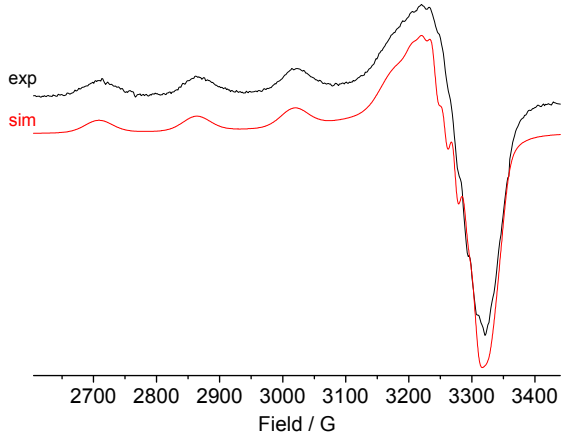

Fig. SI13 X-band EPR spectrum of [Cu(triaz)$_2$] in glassy frozen CH_2Cl_2 solution, recorded at 110 K (upper black line). Simulation with $g_3 = 2.28$, $g_2 = 2.054$, $g_1 = 2.054$, $A_{Cu} = 155$, 15.5, 15.5 G and $A_N = 5$, 14.5, 14.5 G shown below in red.

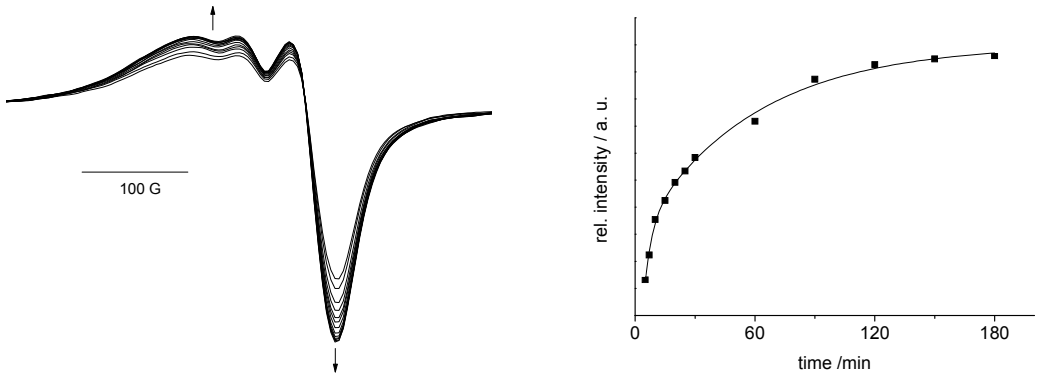

Fig. SI14 X-band EPR spectra recorded on a sample containing 2 eq Htriaz deprotonated with NEt_3 and 1 eq $Cu(OTf)_2$ in 5:3 MeCN/toluene at 298 K (0-60 min). The growth of the signal was

recorded for about 180 min. The rate constant for the underlying unknown reaction was calculated to $k = 5.52 \cdot 10^{-4}\ s^{-1}$ at c = 0.025 $molL^{-1}$ assuming pseudo-first order kinetics. Numerous Cu(II) species can be expected from the following reactions:

$Cu(II)(OTf)_2 + triaz^- \leftrightarrows [Cu(II)(triaz)(OTf)_2]^-$ (a)

$Cu(II)(OTf)_2 + 2\ triaz^- \leftrightarrows [Cu(II)(triaz)_2]$ (b)

$[Cu(II)(triaz)_2] + Cu(II)(OTf)_2 \leftrightarrows [Cu(II)(triaz)_2]^+ + Cu(I)(OTf) + OTf^-$ (c)

$[Cu(II)(triaz)_2]^+ + 2\ NEt_3 \rightarrow [Cu(II)(triaz)(NEt_3)_2] + \ldots$ (d)

…

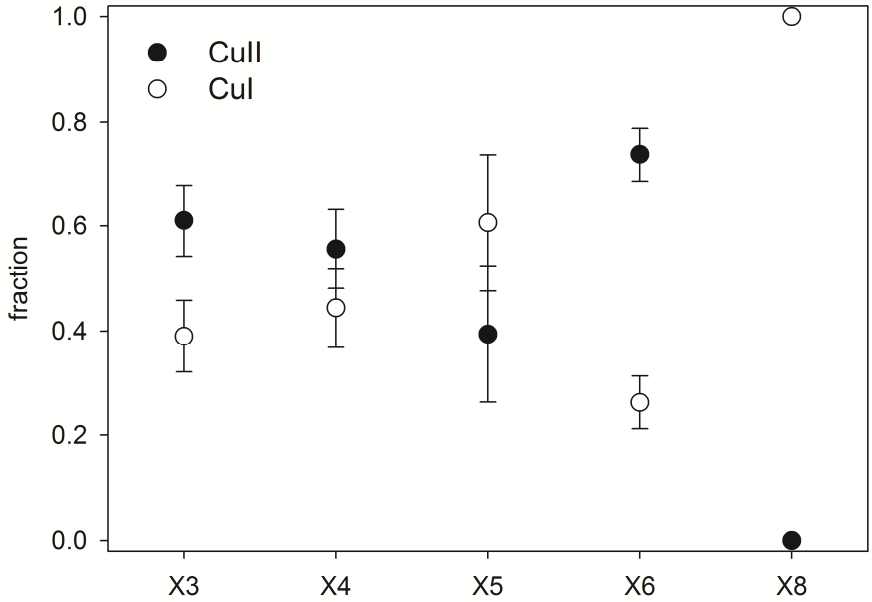

Fig. SI15 Graphic presentation of the LC-XANES fit results. The labels are explained in Table 4.